Performance Calculation of Floating Wind Turbine Tension Leg Platform in the South China Sea

Hai Feng Wang & You Hua Fan

School of Natural Sciences and Humanities, Harbin Institute of Technology Shenzhen Graduate School, Shenzhen, Guangdong province, 518055, China
Email: phdwhf@163.com

Abstract. The harvesting of wind energy is expected to increase greatly in the future because of its stability, abundance, and renewability in large coastal states such as China. The floating support structure will likely become the major structural form for wind turbines in the future due to its cost advantages when the water depth reaches 50 m. The 5MW wind turbine model from National Renewable Energy Lab (NREL) and the modified tension leg platform model proposed by Harbin Institute of Technology (HIT) were applied to certain sea conditions in the South China Sea in order to consider the effects of external load coupling actions. In this study, the internal force, mooring system force, as well as the acceleration, displacement and velocity of the floating structure of the modified HIT Tension Leg Platform (HIT-TLP) were calculated. During this process, the physical parameters of its tension leg structure at a specific frequency domain were obtained to find the technical reserves for its practical application in the future.

Keywords: *acceleration; force; offshore wind turbine; RAOs; structure stress; tension leg platform; velocity.*

1 Introduction

China ranks first in the world for offshore wind resources in the East China Sea and South China Sea along the coast of Guangdong Province. In the South China Sea, however, in most places the water reaches a depth of 50 m. Traditional fixed foundations are too expensive in this type of wind field [1]. As a result, the floating support system is considered a key solution to making offshore wind farms an economical and viable energy resource [2].

There are many existing studies on the tension leg platform of floating offshore wind turbine systems (TLP-FOWTS). The first work on developing a TLP wind turbine system was performed by Withee [3] in 2004 at Massachusetts Institute of Technology. Alina [4], Withee, *et al.* [5], Suzuki [6], Bae, *et al*. [7], Nihei, *et al.* [8], and Bachynski, *et al.* [9] have also done research on tension leg platforms. Jonkman developed a new model to simulate a dynamic offshore floating wind turbine and used it to verify TLP systems [10]. Musial introduced

Received April 22nd, 2015, Revised August 24th, 2015, Accepted for publication September 2nd, 2015.
 ISSN: 2337-5779, DOI: 10.5614/j.eng.technol.sci.2015.47.5.8

an NREL-TLP concept and presented a cost comparison between the Dutch Tri-floater (semi-sub) and the NREL-TLP based on supporting a generic 5-MW wind turbine [11]. Wayman studied several different concepts, including barges and TLPs to support the NREL 5-MW baseline offshore wind turbine [12,13]. Moon, *et al*. [14] provided a general overview of the TLP-type design concept and its environmental and design criteria. Henderson, *et al.* [15] proposed a TLP concept for German waters with the consideration of technological principles, challenges, and potential use as a wind energy resource. In China, research on TLP floating structures for wind turbines is scant. Ren, *et al*. [16,17] introduced a floating structure considering tension leg and mooring lines and also did an experiment to test it. Zhao, *et al.* [18] proposed a new tension leg platform foundation (Wind-Star TLP) for the NREL 5-MW offshore wind turbine and studied motion characteristics under extreme conditions. Wang and Fan designed a new TLP model called the HIT Floating Offshore Wind Turbine-Tension Leg Platform (HIT-FOWT-TLP) [19].

The HIT-TLP model with a 5-MW wind turbine model from NREL, proposed by Harbin Institute of Technology (HIT) in [19], was adopted in this paper. We first conducted a response amplitude operator calculation, thus obtaining the external additional coupling loads on the tension leg platform by calculating the external force transmitted by fluid-solid coupling, and subsequently calculated the acceleration, displacement, velocity, and force in the structure.

2 Analysis Input

2.1 NREL 5MW Wind Turbine Model

The NREL 5 MW offshore wind turbine was used in this study. It was designed by Jonkman as a preliminary concept [20]. The NREL 5 MW baseline is a conventional up-wind machine with three blades operating at variable speeds and pitches.

2.2 HIT-TLP Model

The HIT-TLP model was created by H.F. Wang and Y.H. Fan [19] and is called the HIT Floating Offshore Wind Turbine Tension Leg Platform (HIT-FOWT-TLP) in order to distinguish it from other types of platforms. The unique features of the HIT-FOWT-TLP are its single column with four pontoons and its 5 m high bevel-shaped free board. Larger diameters are considered for the spokes and the connection between the spokes and the column is welded. The platform diameter is 14 m and the platform draft diameter is 30 m. The distance between the fairleads is 48 m and the concrete height is 13 m, which is different from the initial design because the design center and the water depth are the

same as those of the MIT model at 200 m. A three-dimensional image of the modified HIT-TLP model is shown in Figure 1.

Figure 1 Modified HIT-TLP model.

2.3 Environment and Site Data

Environmental conditions from previous research were used [19]. An average installation site depth of 200 m was considered here. A wave spectrum is the distribution of wave energy as a function of frequency, which describes the total energy transmitted by a wave field at a specific time. The energy density of the wave is defined by the Pierson-Moskowitz spectrum [19]:

$$S(\omega) = \pi^3 (\frac{2H_S}{T_z^2})^2 \frac{1}{\omega^5} \exp[-\pi^3 (\frac{2}{T_z \omega})^4] \quad (1)$$

where ω is the wave frequency, H_S is the significant wave height, and T_z is the zero-crossing period.

3 FEM Model

In the calculation model, the water depth in the computational domain adopted was 200 m and the core computational domain had a radius of 300 m. The internal structure was designed to adopt the middle reinforcement mode. The TLP, 0.02 m thick, is arranged with inclined stiffening ribs at 30° on the top, while 600 mm thick reinforcing ribs are mounted on the upper part of the contact between the inclined stiffening ribs and the tower. The main pontoon has a thickness of 0.02 m and is reinforced with 600 mm thick horizontal stiffening ribs at an interval of 5 m inside and 600 mm thick stiffening ribs at an interval of 90° vertically. The auxiliary pontoon, with thickness 0.03 m, uses a circular cross-section. Environmental load and external force were applied and kept constant as above. Three-dimensional images are shown in Figures

2a, b and c, while the water and mesh are shown in Figure 3 and Figure 4 respectively.

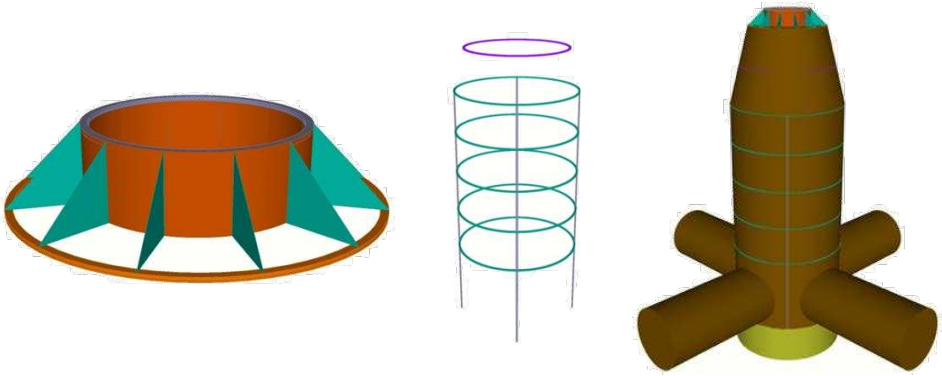

(a) Top inclined and horizontal stiffening ribs

(b) Internal horizontal and vertical stiffening ribs

(c) Integral structure model

Figure 2 Three-dimensional images.

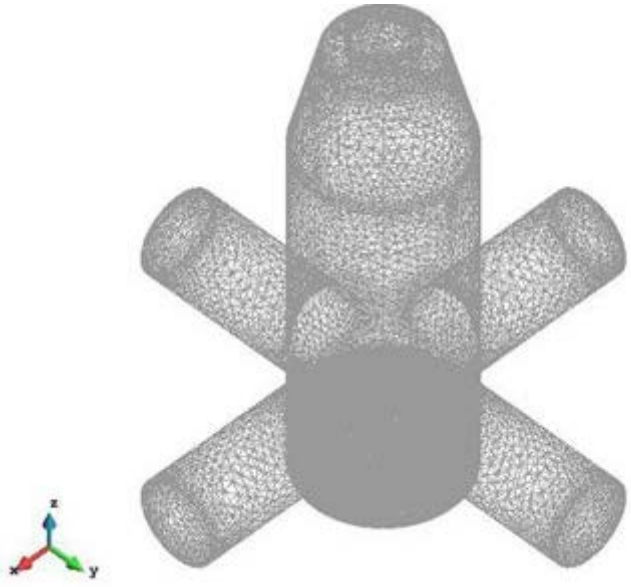

Figure 3 Mesh generation.

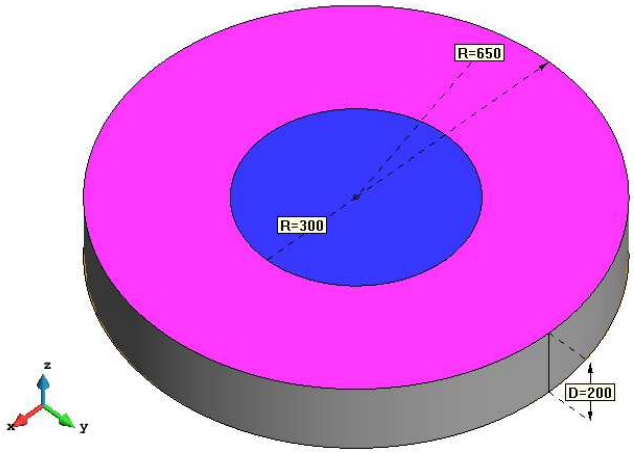

Figure 4 Calculated waters.

4 Calculation and Analysis

4.1 Response Amplitude Operator (RAO) Calculation

The response amplitude operator (RAO) is defined as the response of a floating structure in a given mode of motion to a wave of unit amplitude as a function of frequency [21]. The RAOs of the rotation degree are normalized by the platform length. Figures 5 to 10 show that the RAO results in the yaw, roll, and pitch directions were relatively low. Therefore, the dynamic responses in these directions were not taken into consideration under such loads.

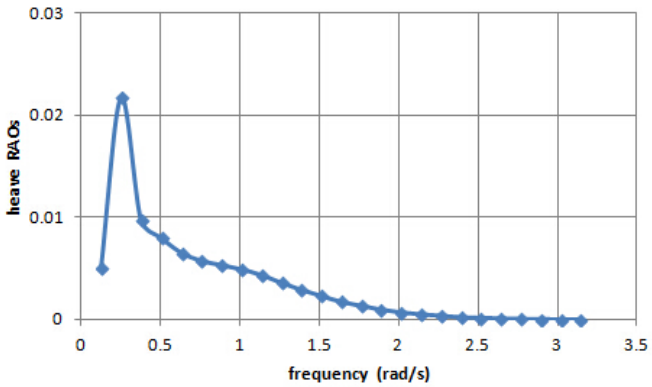

Figure 5 Heave RAOs.

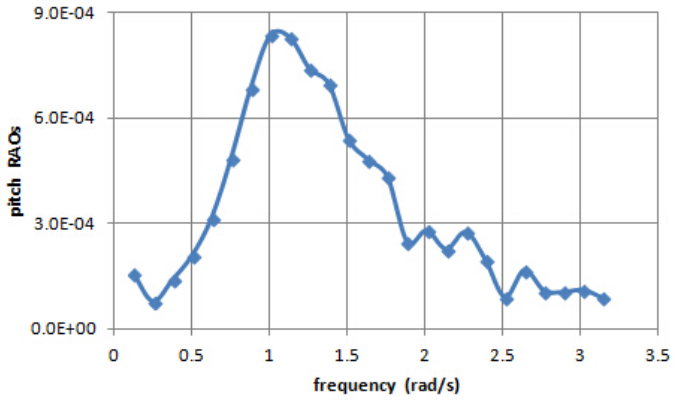

Figure 6 Pitch-RAOs.

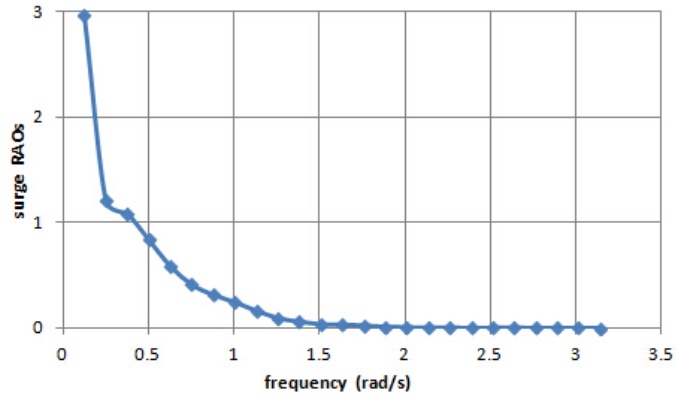

Figure 7 Surge RAOs.

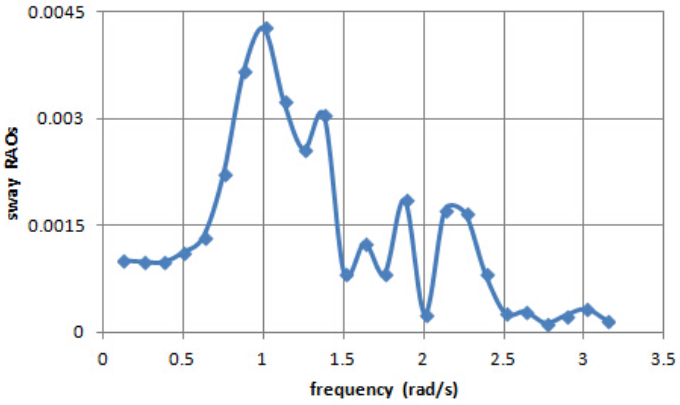

Figure 8 Sway-RAOs.

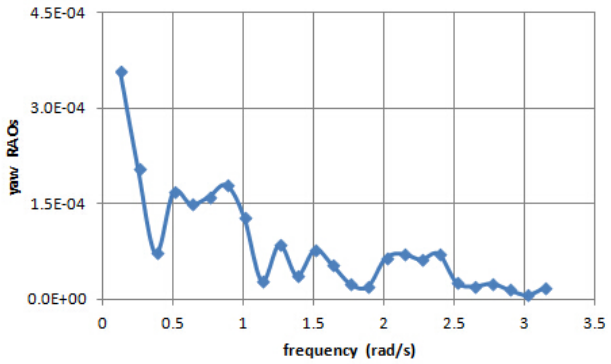

Figure 9 Yaw RAOs

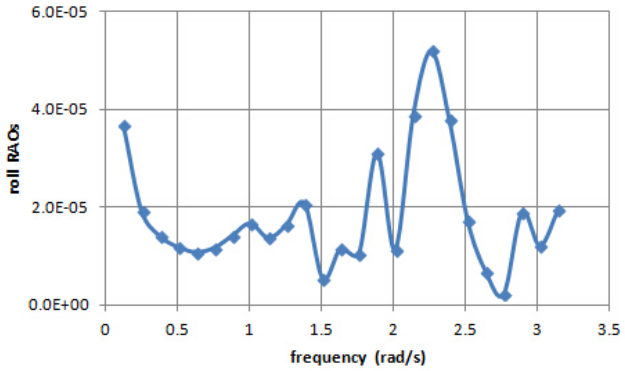

Figure 10 Roll-RAOs

Figures 5-10 show that the RAO results in the yaw, roll, and pitch directions were relatively low, therefore, the dynamic responses in these directions were not taken into consideration under such loads. Secondly, amplitude varied greatly in the sway direction and the maximum RAO result appeared at 1.0 rad/s, i.e. 6.28 s. The maximum RAO response appeared in the surge direction, i.e. a relatively large dynamic response appeared between 0 and 6.28 s.

4.2 Structural Stress Results

The maximum integral structure stress appeared at the contact of the four auxiliary pontoons with the main pontoon (20 Mpa), as shown in Figure 11, lower than the design strength. The stress results meet the use requirements but there is potential for optimization. As the main pontoon is within the range of relatively low strength, concrete was used inside as ballasting and as an internal supporting structure to reduce the stress effects on the internal structure. In the

calculation of the internal structure stress, the stress results which are shown in Figure 12 also meet the design requirements and but there is room for optimization.

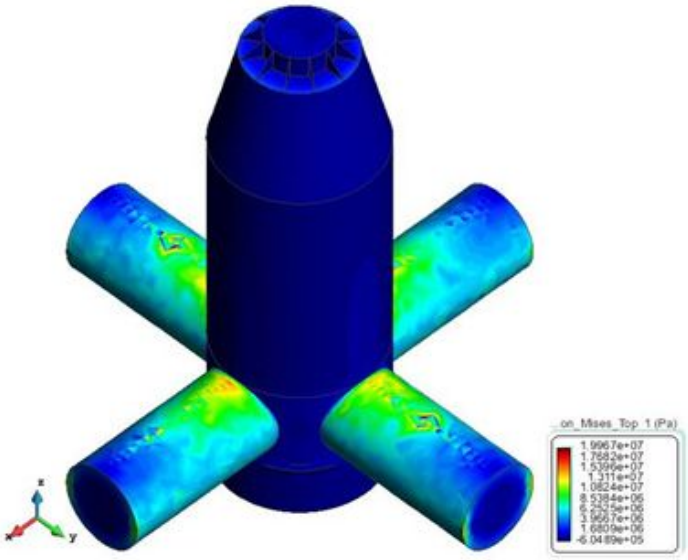

Figure 11 Structure stress.

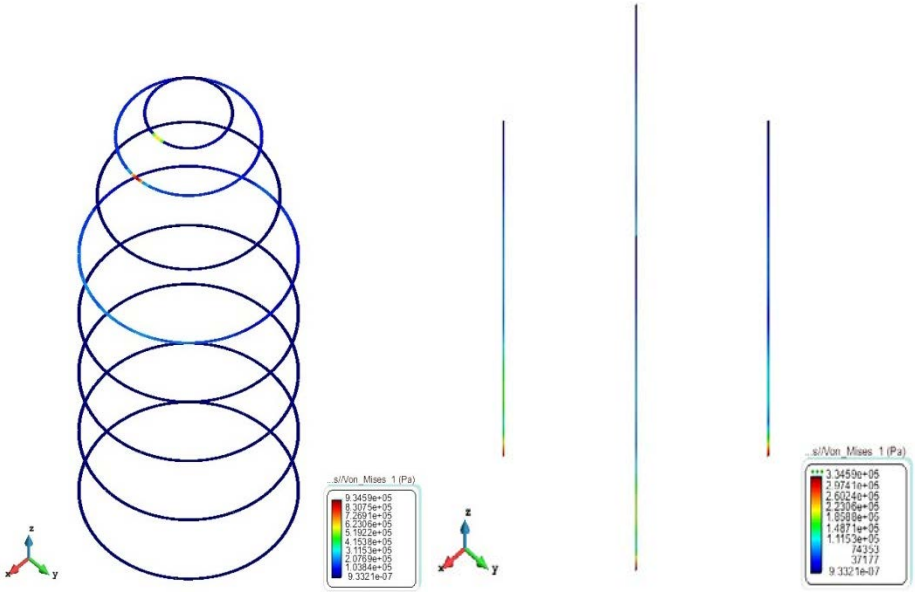

Figure 12 Internal structural stress.

4.3 Force Analysis for Mooring System

The mooring system under the action of an external periodic force, N, within 60 s was calculated and the results were as shown in Figures 13-18. The force change was minimal, with 30 N as the maximum in the Y direction vertical to the external force, i.e. the sway direction. This is mainly because the external force was applied vertically in the Y direction, where there is no deflection. The X direction was subjected to direct external force, yielding a maximum internal force of 9.0E5 N. The mooring system was tensioned in the Z direction, yielding an internal force of 2.3E7 N. The maximum bending moment (1.4E7 N) appeared at MY.

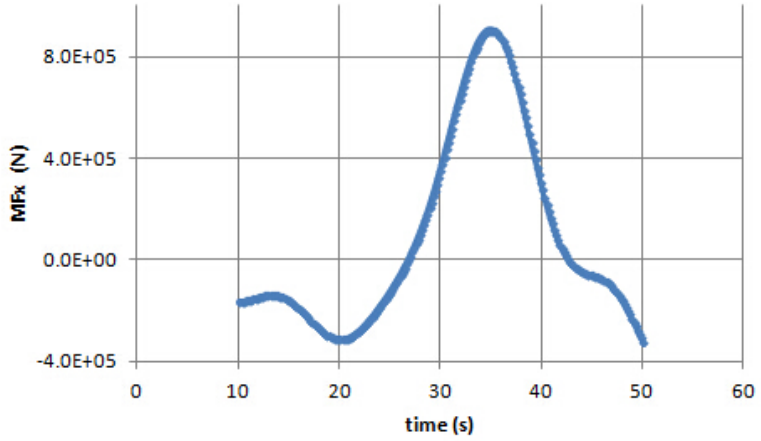

Figure 13 Mfx – Time.

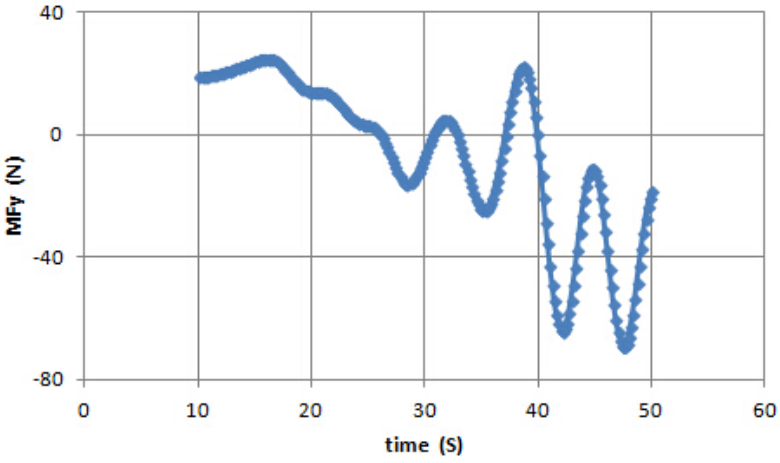

Figure 14 Mfy – Time.

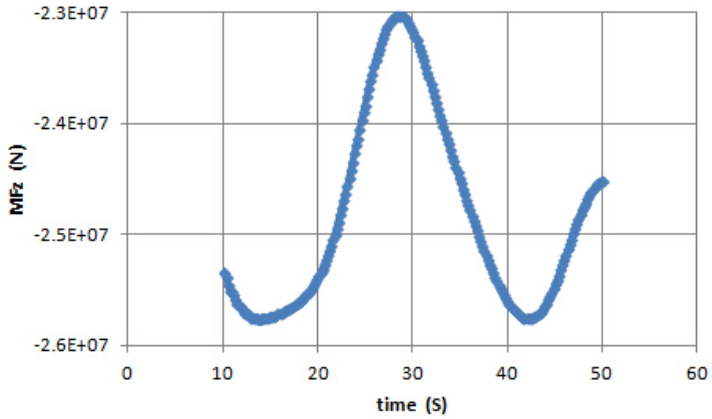

Figure 15 Mfz – Time.

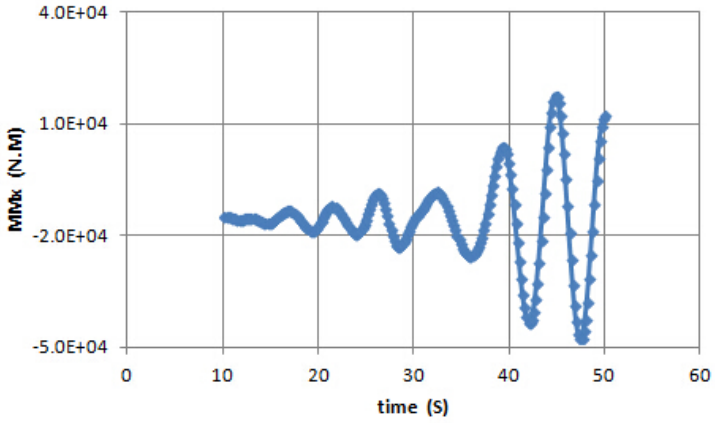

Figure 16 Mx – Time.

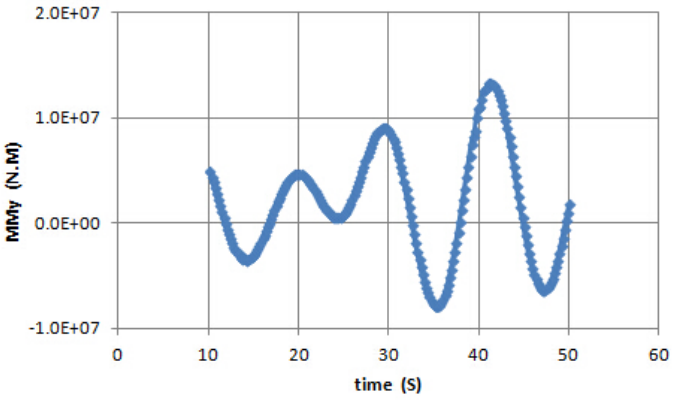

Figure 17 My – Time.

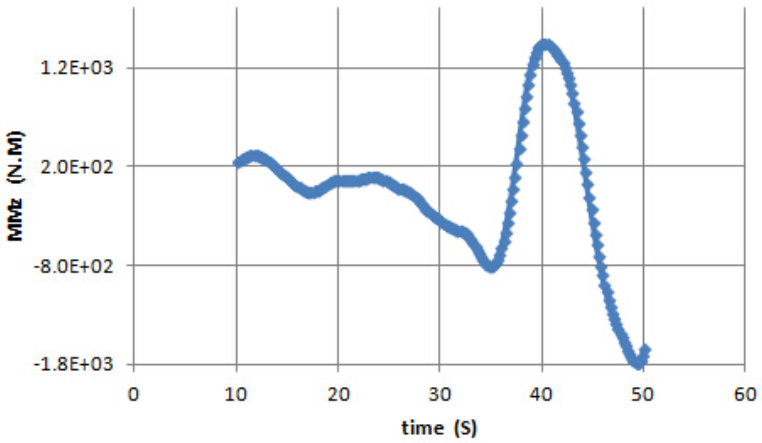

Figure 18 Mz – Time.

4.4 Integral Displacement Calculation and Analysis

The displacement and rotation calculation results under external periodic force N are shown in Figures 19-22, with only 60 s taken into consideration. In the heave movement in Figure 19, the maximum displacement amplitude was between 30 and 40 s, and the displacement at other intervals was generally in the same range. Though the time period selected was relatively short, the subsequent change was consistent with that in the period of 60 s. The rotation angle changed from 2E-5 to -3E-5 in the pitch direction, with the maximum rotation angle appearing at about 40 s.

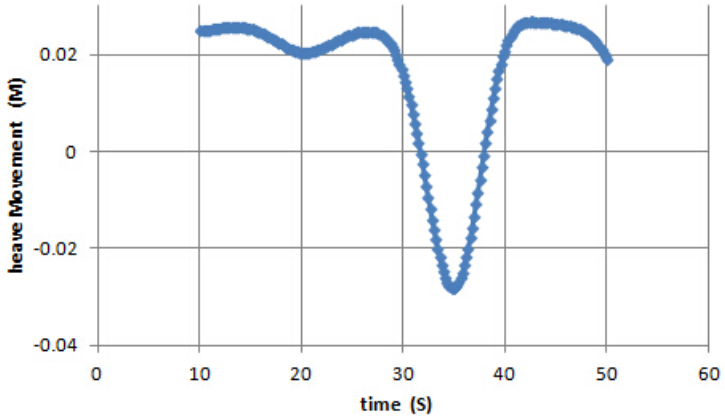

Figure 19 Heave movement – Time.

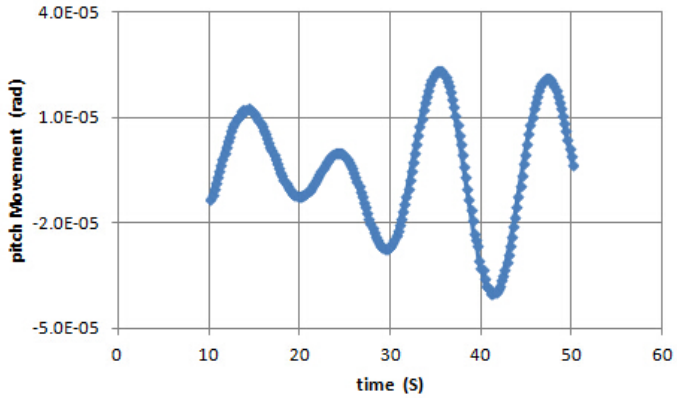

Figure 20 Pitch movement – Time.

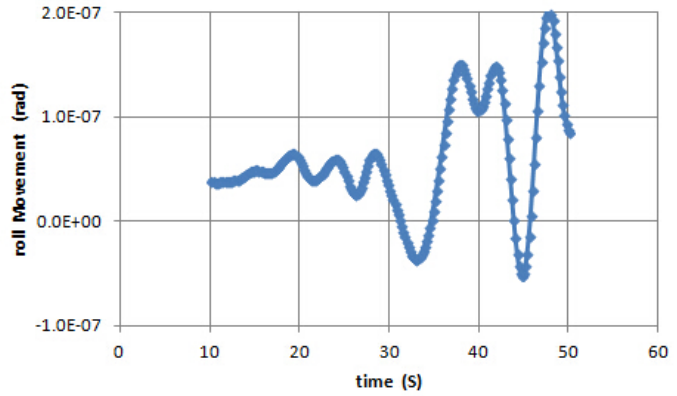

Figure 21 Roll movement – Time.

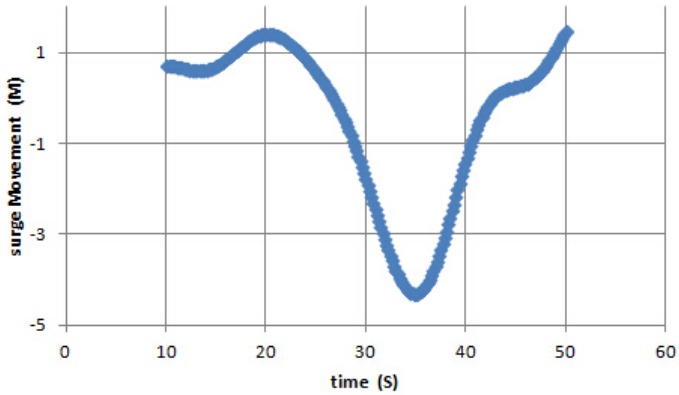

Figure 22 Surge movement – Time.

The angle changed from 2E-7 to -0.5E-7 in the roll direction in Figure 21, with the maximum result appearing at the interval close to 50 s. The displacement change in Figure 22 is relatively large, from 1.5 to 4 m in the surge direction as it was subjected to direct external loads, with a maximum displacement of 4 m appearing at the time interval 30-40 s.

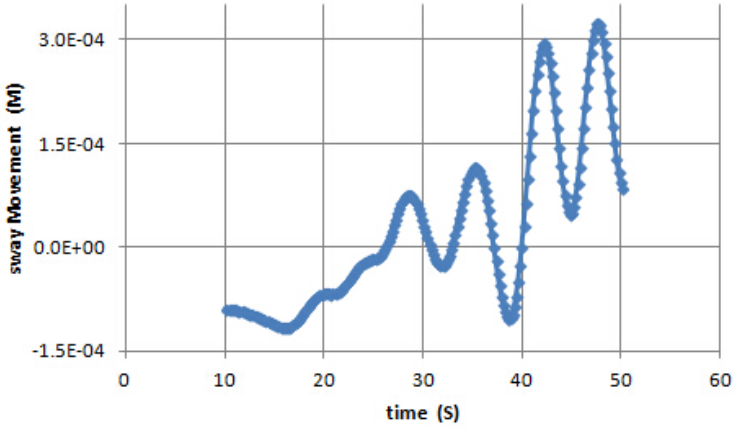

Figure 23 Sway movement – Time.

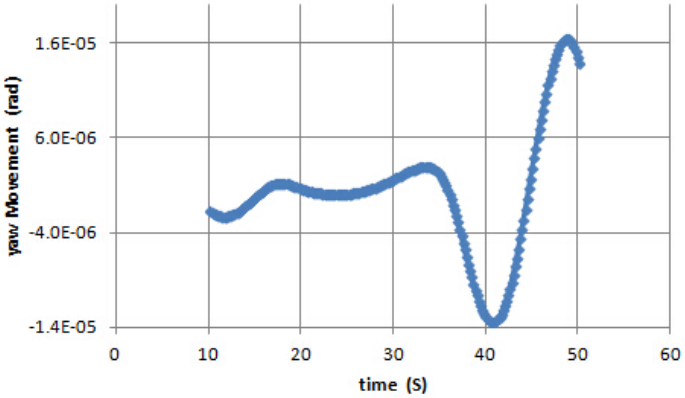

Figure 24 Yaw movement – Time.

In the sway and yaw direction in Figure 23 and Figure 24, the change range was from -1.5E-4 to 3.0E-4, with a maximum displacement appearing at 50 s, as a result of the relatively large amplitude but very small displacement value of about 0.3 m, which may be neglected when compared with that in the surge direction. The angle changed from -1.4E-5 to 1.6E-5 in the yaw direction, with a maximum result of 1.6E-5 appearing at about 50 s.

4.5 Calculation and Analysis of Overall Acceleration and Velocity

4.5.1 Acceleration Analysis

Under the action of an external periodic force of 846.26 kN, the overall acceleration calculation results were as shown in Figure 25-30, only taking 60 s into consideration. In the heave direction in Figure 25, the maximum acceleration appeared between 30 s and 40 s where the displacement changed relatively greatly with a maximum of 0.008 m/s^2; in the pitch direction in Figure 26, the maximum acceleration of 2E-4 appeared at 40 s. The acceleration was relatively low; in the roll (in Figure 27), sway (in Figure 29), and yaw (in Figure 30) directions it may be neglected. In the analysis focusing on the acceleration in the surge direction most external forces were found, as can be seen in Figure 28. The maximum exceeded 0.3 m/s^2.

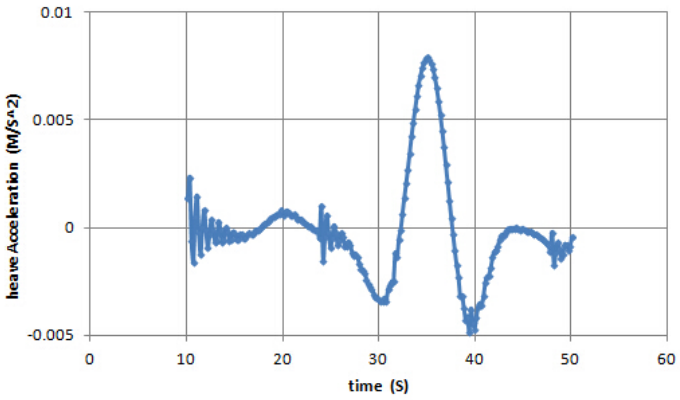

Figure 25 Heave acceleration – Time.

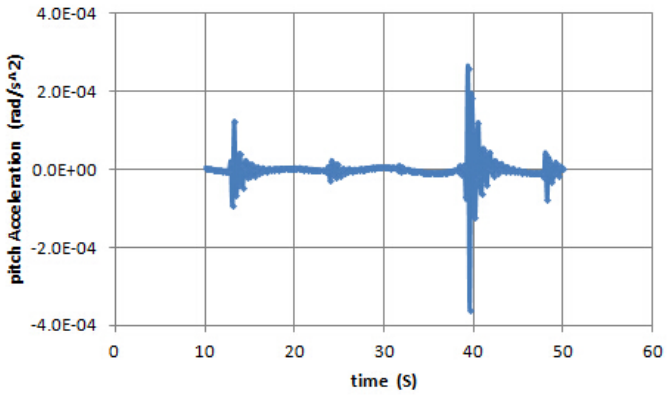

Figure 26 Pitch Acceleration – Time.

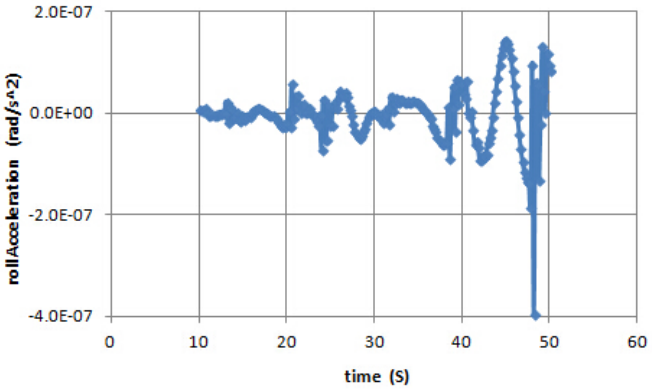

Figure 27 Roll Acceleration – Time.

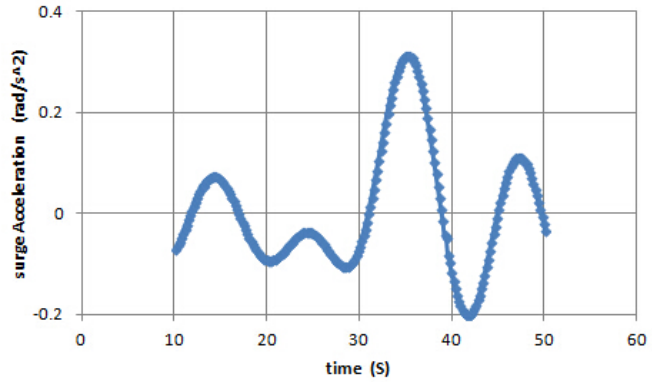

Figure 28 Surge Acceleration – Time.

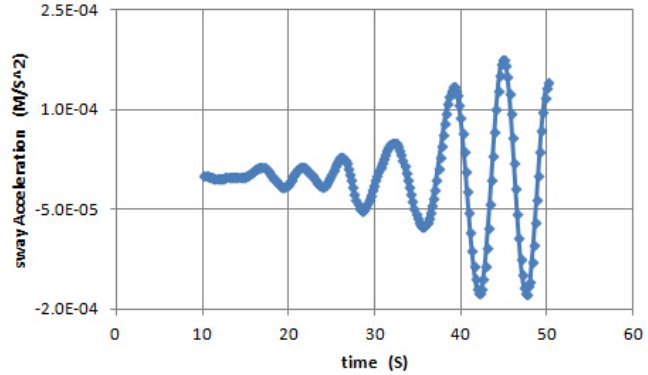

Figure 29 Sway Acceleration – Time.

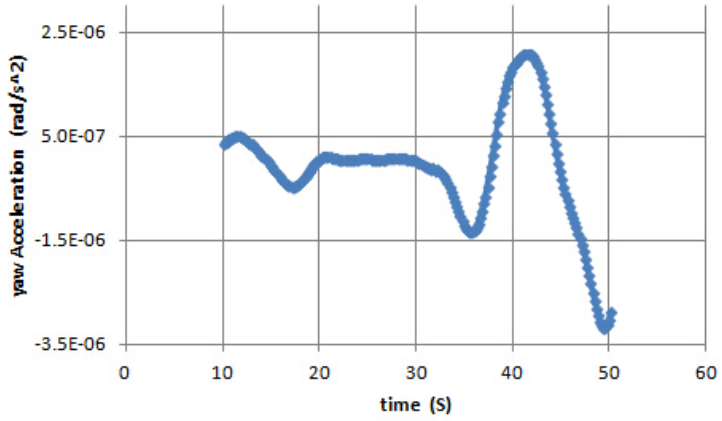

Figure 30 Yaw Acceleration – Time.

4.5.2 Velocity Analysis

The speed variation trend was similar to that of acceleration and displacement. The amplitude in the surge direction in Figure 34 and heave direction in Figure 31 is far beyond the variation trends in the other directions, which are shown in Figure 32, Figure 33, Figure 35 and Figure 36. The maximum speed was 0.015 m/s in the heave direction, as shown in Figure 31, and the maximum result exceeded 0.7 m/s in the surge direction, as shown in Figure 34.

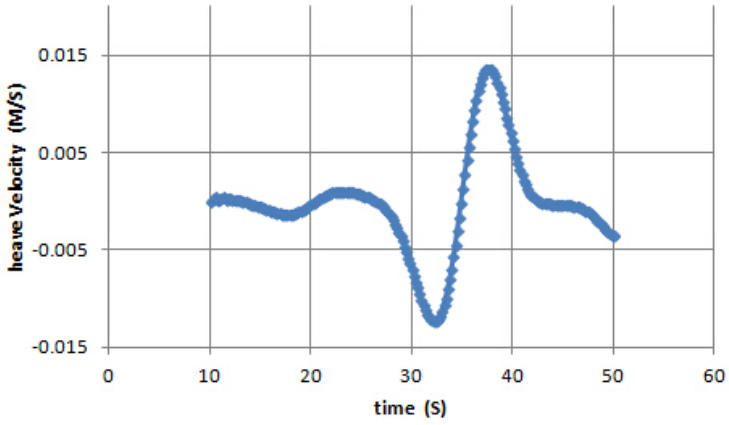

Figure 31 Heave Velocity – Time.

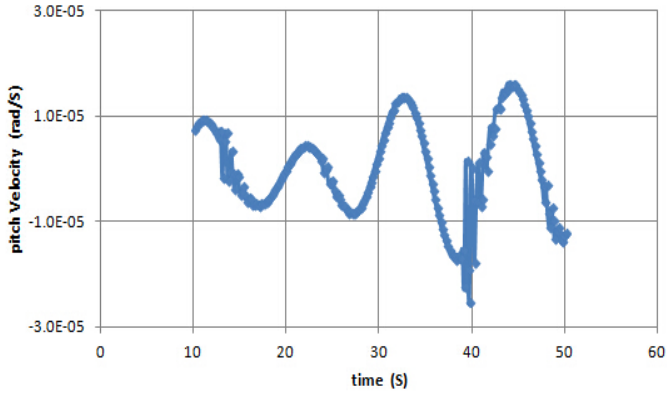

Figure 32 Pitch Velocity – Time.

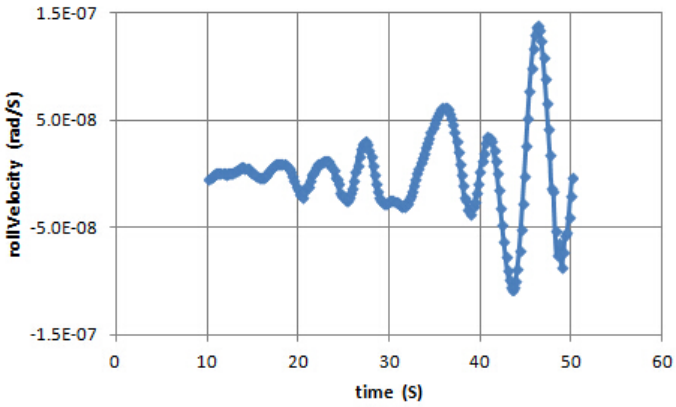

Figure 33 Roll Velocity – Time.

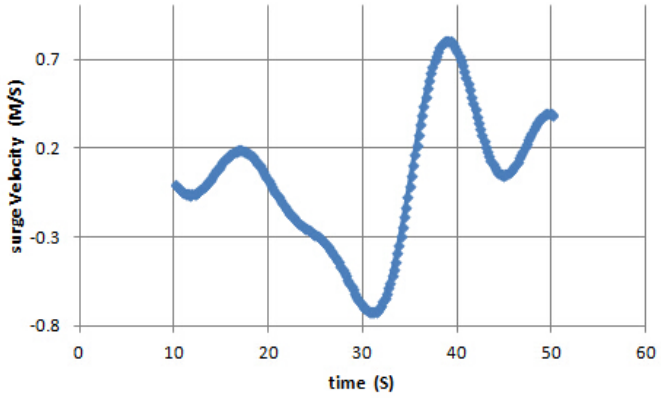

Figure 34 Surge Velocity – Time.

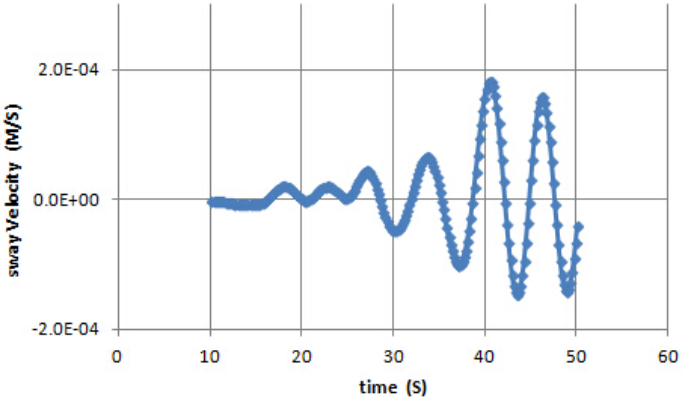

Figure 35 Sway Velocity – Time.

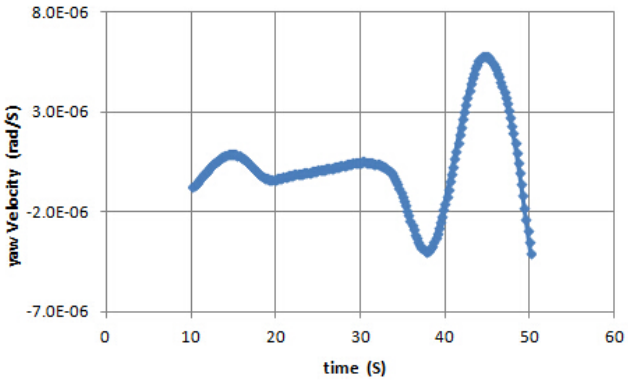

Figure 36 Yaw Velocity – Time.

5 Conclusions

In this study we have calculated and analyzed integral structure internal force, mooring system force, as well as acceleration, displacement, and velocity for a modified tension leg to consider the combined effects of wind-wave-current, using a modified TLP model proposed by Harbin Institute of Technology (HIT) with a 5-MW wind turbine model from NREL.

Within the range of the frequency domain, RAOs were calculated in different directions respectively. The RAOs results in the yaw, roll, and pitch directions were relatively low and can be neglected. The maximum RAO response appeared in the surge direction. When considering the structure stress, the maximum integral structure stress appeared at the contact of the four auxiliary pontoons with the main pontoon (20 Mpa), below the design strength. Since

concrete is used inside as the ballasting and internal supporting structure, the main pontoon is within the range of relatively low strength, and the stress results also meet the design requirements, while there is still room for optimization.

To the force and mooring system, the change was minimal, with 30 N as the maximum in the sway direction vertical to the external force. The surge direction was subjected to direct external force, yielding a maximum internal force of 9.0E5 N. The mooring system was tensioned in the heave direction, yielding an internal force of 2.3E7 N.

Considering the displacement in different directions, in the heave direction, the maximum displacement amplitude appeared between 30 s and 40 s, and the displacement at other intervals generally remained in the same range. The displacement change was relatively large, from 1.5 m to 4 m in the surge direction as it was subjected to direct external loads, with a maximum displacement of 4 m appearing in the time interval of 30-40 s. In the heave direction, the maximum acceleration appeared between 30 s and 40 s where displacement changed relatively greatly with a maximum at 0.008 m/s2. Acceleration in the surge direction was an analysis focus where most external forces were found. The maximum exceeded 0.3 m/s2. The speed variation trend was similar to that of acceleration and displacement. The amplitude in the surge and heave directions was far beyond the variation trend in the other directions. The maximum speed was 0.015 m/s in the heave direction and the maximum result exceeded 0.7 m/s in the surge direction. Displacement, acceleration, and speed were relatively low in the roll, sway, and yaw directions, and may be neglected.

References

[1] Wang, H.F. & Fan, Y.H., *Preliminary Design of Offshore Wind Turbine Tension Leg Platform in the South China Sea*, Journal of Engineering Science and Technology Review, **6**(3), pp. 88-92, 2013.

[2] Jonkman, J.M., *Dynamics Modeling and Loads Analysis of an Offshore Floating Wind Turbine,* 2007.

[3] Withee, J.E., *Fully Coupled Dynamic Analysis of a Floating Wind Turbine System,* PhD Dissertation, Naval Postgraduate School, Monterey, California, 2004.

[4] Alina, C., *Design and Dynamic Modeling of the Support Structure for a 10 MW Offshore Wind Turbine*, Master thesis, Norwegian University of Science and Technology, Trondheim, Norway, 2011.

[5] Withee, J.E. & Sclavounos, P.D., *Fully Coupled Dynamic Analysis of a Floating Wind Turbine System,* in Proceedings of the 8th World Renewable Energy Congress, 2004.
[6] Suzuki, K., *Development of TLP Type Floating Structure for Offshore Wind Farms,* Technical Report, Mitsui Engineering and Shipbuilding Co., Ltd: Japan, 2009.
[7] Bae, Y.H., Kim, M.H. & Shin, Y.S., *Rotor-floater Mooring Coupled Dynamic Analysis of Mini TLP-type Offshore Floating Wind Turbines.* in Proceedings of the 29th International Conference on Ocean, Offshore and Arctic Engineering, 2010.
[8] Nihei, Y. & Fujioka, H., *Motion Characteristics of a TLP Type Offshore Wind Turbine in Waves and Win,* in Proceedings of the 29th International Conference on Ocean, Offshore and Arctic Engineering, 2010.
[9] Bachynski, E.E. & Torgeir, M., *Design Considerations for Tension Leg Platform Wind Turbines,* Marine Structures, **29**, pp. 89-114, 2012.
[10] Jonkman J.M., *Dynamics of Offshore Floating Wind Turbines – Model Development and Verification,* Wind Energy, **12**(5), pp. 459-492, 2009.
[11] Musial, W., Butterfield, S. & Boone, A., F*easibility of Floating Platform Systems for Wind Turbines*, NREL/CP-500-34874, 2003.
[12] Wayman, E., *Coupled Dynamics and Economic Analysis of Floating Wind Turbine Systems,* Master Thesis, Massachusetts Institute of Technology, 2006.
[13] Wayman, E.N., Sclavounos, P.D., Butterfield, S., Jonkman, J. & Musial, W., Offshore Technology Conference, Houston, Texas, 1-4 May, 2006, Paper No. OTC 18287.
[14] Moon, W.L. & Nordstrom, C.J., *Tension Leg Platform Turbine: A Unique Integration of Mature Technologies,* in Proceedings of the 16th Offshore Symposium, Texas Section of the Society of Naval Architects and Marine Engineers (ed(s)), 2010.
[15] Henderson, A.R., Argyriadis, K., Nichols, J. & Langston, D., *Offshore Wind Turbines on TLPs – Assessment of Floating Support Structures for Offshore Wind Farms in German Waters,* in Proceedings of 10th German Wind Energy Conference, 2010.
[16] Ren, N., Li, Y. & Ou, J., *The Effect of Additional Mooring Chains on the Motion Performance of a Floating Wind Turbine with a Tension Leg Platform,* Energies, **5**(4), pp. 1135-1149, 2010.
[17] Ren, N., Li, Y. & Ou, J., *The Wind-wave Tunnel Test of a Tension-leg Platform Type Floating Offshore Wind Turbine,* Journal of Renewable and Sustainable Energy, **4**(6), pp. 063117, 2012.
[18] Zhao, Y.S., Jian, M.Y. & Yan, P.H., *Preliminary Design of a Multi-column TLP Foundation for a 5-MW Offshore Wind Turbine,* Energies, **5**, pp. 3874-3891, 2012.

[19] Wang, H.F., Fan, Y.H. & Liu, Y., *Dynamic Analysis of a Tension Leg Platform for Offshore Wind Turbines,* Journal of Power of Technologies, **94**, pp. 42-49, 2014.
[20] Jonkman, J.M., Butterfield S., Musial W. & Scott G., *Definition of a 5-MW Reference Wind Turbine for Offshore System Development*, National Renewable Energy Laboratory: Colorado, USA, 2009.
[21] Matha, D., *Model Development and Loads Analysis of an Offshore Wind Turbine on a Tension Leg Platform with a Comparison to Other Floating Turbine Concepts: April 2009*, National Renewable Energy Laboratory (NREL), Golden, CO., 2010.